Photoacoustics 28 (2022) 100418

Contents lists available at ScienceDirect

Photoacoustics

journal homepage: www.elsevier.com/locate/pacs

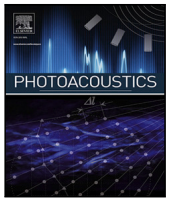

Research article

Assessment of prostate cancer progression using a translational needle photoacoustic sensing probe: Preliminary study with intact human prostates *ex-vivo*

Linyu Ni [a], Wei-kuan Lin [b], Amy Kasputis [c], Deborah Postiff [d], Javed Siddiqui [d], Matthew J. Allaway [e], Matthew S. Davenport [c,f], John T. Wei [c], Jay L. Guo [b], Todd M. Morgan [c], Aaron M. Udager [g], Xueding Wang [a,f,*], Guan Xu [a,h,**]

[a] Department of Biomedical Engineering, University of Michigan, 500 S. State St., Ann Arbor, 48109, MI, USA
[b] Department of Electrical Engineering and Computer Sciences, University of Michigan, 500 S. State St., Ann Arbor, 48109, MI, USA
[c] Department of Urology, University of Michigan, 500 S. State St., Ann Arbor, 48109, MI, USA
[d] Department of Pathology, University of Michigan, 500 S. State St., Ann Arbor, 48109, MI, USA
[e] Perineologic, 183 N Centre Street, Cumberland, 21502, Md, USA
[f] Department of Radiology, University of Michigan, 500 S. State St., Ann Arbor, 48109, MI, USA
[g] Michigan Center for Translational Pathology, Rogel Cancer Center, Department of Pathology, University of Michigan, 500 S. State St., Ann Arbor, 48109, MI, USA
[h] Department of Ophthalmology and Visual Sciences, University of Michigan, 500 S. State St., Ann Arbor, 48109, MI, USA

ARTICLE INFO

Keywords:
Photoacoustic spectral analysis
Prostate cancer
The translational photoacoustic sensing needle probe

ABSTRACT

In our previous studies, we demonstrated the ability of an interstitial all-optical needle photoacoustic (PA) sensing probe and PA spectral analysis (PASA) to assess the aggressiveness of prostate cancer. In this clinical translation investigation, we integrated the optical components of the needle PA sensing probe into a 18G steel needle. The translational needle PA sensing probe was evaluated using intact human prostates in a simulated ultrasound-guided transperineal prostate biopsy. PA signals were acquired at 1220 nm, 1370 nm, 800 nm and 266 nm at each interstitial measurement location and quantified by PASA within the frequency range of 8–28 MHz. The measurement locations were stained for establishing spatial correlations between the quantitative measurements and the histological diagnosing. Most of the quantitative PA assessments reveal statistically significant differences between the benign and cancerous regions. Multivariate analysis combining the PASA quantifications shows an accuracy close to 90% in differentiating the benign and cancerous regions in the prostates.

1. Introduction

The standard diagnosis approach of prostate cancer (PCa) is needle-based core biopsy guided by transrectal ultrasound (TRUS). Histopathologic processing of the extracted tissue visualizes the microscopic architecture of the tissue, which reflects the aggressiveness of the PCa [1]. TRUS guided prostate biopsy has a poor core yield and a high false negative rate owing to TRUS's limited sensitivity to PCa and the small volume of the biopsy core [2]. Magnetic resonance imaging (MRI) TRUS fusion biopsy has recently been introduced as a method to improve the identification of the clinically significant PCa in patients with initial negative biopsies [3–5]. Nonetheless, the procedure requires the fusion of MRI and Ultrasound (US) imaging that is subject to registration and targeting error.

Photoacoustic (PA) imaging and sensing, taking advantage of the unique optical absorption profiles of tissue components, is able to acquire microscopic tissue architecture at US resolution [6]. Our previous studies validated that the frequency domain analysis of the photoacoustic signal power distribution, namely PA spectral analysis (PASA), can statistically quantify the content and microarchitectural distribution of tissue components inside the tissue-volume-of-interest [7]. Recent studies using human and animal prostates, including those by our [8,9] and other groups [10,11] have demonstrated that PASA can differentiate between benign and cancerous prostate tissues, and assess the

* Corresponding author at: Department of Biomedical Engineering, University of Michigan, 500 S. State St., Ann Arbor, 48109, MI, USA.
** Corresponding author at: Department of Ophthalmology and Visual Sciences, University of Michigan, 500 S. State St., Ann Arbor, 48109, MI, USA.
E-mail addresses: xdwang@umich.edu (X. Wang), guanx@umich.edu (G. Xu).

https://doi.org/10.1016/j.pacs.2022.100418
Received 12 August 2022; Received in revised form 17 October 2022; Accepted 23 October 2022
Available online 28 October 2022

aggressiveness of PCa. Therefore, PASA technology holds the promise to provide a diagnosis of PCa *in situ* without the need for tissue extraction, and may reduce the amount of biopsy core extractions and post-core-biopsy complications [12].

Encoding fine microarchitecture information comparable to histology, high frequency PA signal components attenuate fast through the biological tissue [13]. Aimed at capturing these high frequency signal components, we recently developed an interstitial PA measurement approach [8]. The interstitial measurement instrumentation includes a fiber optic diffuser for illumination and a needle hydrophone for signal detection. When joined together, the two components possess a slim profile for insertion into the prostate and allow for broadband PA signal acquisition from the surrounding tissue. The approach has been validated in detecting the progressive PCa in prostate tissue blocks [14] and intact prostates from human subjects *ex vivo* [8] and animals *in vivo* [9]. Our latest work further miniaturized the interstitial needle PA sensing probe with an all-optical design that consists of a fiber optic diffuser and a fiber optic hydrophone [14].

In this study, we integrated the all-optical components into the inner lumen of a steel needle with the dimension close to a core-biopsy needle with the purpose of clinical translation. The mechanical reliability of the needles was examined by a certified medical device testing company (DDL, Inc., Eden Prairie, MN). The performance of the translatable needle PA sensing probe was examined in a simulated TRUS guided transperineal biopsy procedure using intact human prostates procured through radical prostatectomies. When inserted into the prostate, the needle PA sensing probe collected PA signals at multiple wavelengths targeting a series of tissue components. The measurement locations were stained by dye injection so that the histopathology results from the same locations can be compared to the PASA quantifications.

2. Method

2.1. Translational needle PA sensing probe

The needle PA sensing probe, as shown in Fig. 1, included an 800 μm-diameter fiber diffuser for light illumination, a 150 μm-diameter fiber optic hydrophone for US detection, and a 200 mm-long 18G medical needle (TruGuide, Bard Peripheral Vascular Inc, Tempe, AZ). The emission segment of the fiber optic diffuser has a length of 6 mm and a conical shape, as shown in Fig. 1(a). The detailed fabrication procedures of the fiber diffuser were described in [15] and our earlier study [14]. The fiber optic hydrophone with a plano-concave microresonator at the detection end [16] was driven by a commercial fiber optic hydrophone data acquisition system (Precision Acoustics, UK). The functional segments of both the fiber optic diffuser and the fiber optic hydrophone were exposed through a 12 mm-long side-view window at the end of the 18G medical needle, as shown in Fig. 1. The 12 mm length was chosen because the prostate biopsy core is 12 mm in length. The window cutout possessed introducing angles, as shown in Fig. 1(b), to prevent resistance during needle insertion and withdrawal. The inner surface of the side-view window was coated with gold for optimal illumination efficiency, as shown in Fig. 1(c).

2.2. Simulated TRUS guided transperineal needle PA sensing probe insertion procedure

This study simulated a TRUS guided transperineal biopsy procedure [17] using intact human prostates *ex vivo*. The protocol for procuring the prostate after prostatectomy procedures and using the prostates in our experiments was approved by the Institutional Review Board of the University of Michigan Medical School. All subjects provided written informed consents. Fig. 2 depicts the experiment setup, and the procedures are explained below.

In the simulated system in Fig. 2, the 2D imaging plane of an endocavity US array (E9-4, Zonare, Mountain View, CA) was aligned

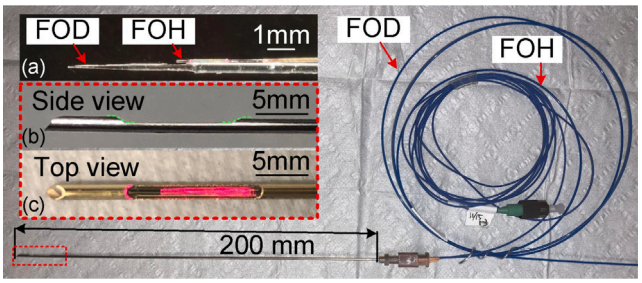

Fig. 1. The needle PA sensing probe. (a) Optical components. FOD: Fiber optic diffuser. FOH: Fiber optic hydrophone. (b) Side view and (c) Top view of the needle probe in the red-dashed box in (a). The green dashed line marks the introducing angles. 700 nm laser was coupling into the illumination fiber in (c).

with a biopsy template with evenly distributed sampling holes for the needle PA sensing probe. Before the experiment, the sampling track in US imaging corresponding to each sampling hole were determined, as illustrated in Fig. 3. A silicone rubber mold (Ecoflex 00-30, Smooth-On Inc., Macungie, PA) imitating the skin and subcutaneous tissue in the perineal region was used to seal the human prostate. The rubber mold containing the prostate was secured underneath the positioning system. The US array was coupled to the surface of the rubber mold with US gel. By rotating the holder attached to the US array, the US field-of-view can cover the whole prostate volume. Most of the prostatectomy patients went through preprocedural MRI. The MRI reports provided the approximate locations of the benign and cancerous regions. Along with the prostate contour shown in the TRUS imaging, we can have samplings targeting either the benign or the cancerous region. Once a needle insertion location was determined through US imaging, an 14G introducer needle (PrecisionPoint, Perineologic, Cumberland, MD) used in regular biopsy procedure were inserted through the sampling template into the rubber mold and made a pathway for the needle PA sensing probe. The needle PA sensing probe was then inserted to the desired location inside the prostate guided by the needle position presented in the real-time US imaging, as illustrated by Fig. 3 and the supplemental video. During the operations, TRUS was only to identify the contour of the prostate and monitor the position of PA sensing probe during insertion.

The outputs of an optical parametric oscillator (OPO) pumped by the second harmonic of an Nd:YAG laser (Phocus Mobile, OPOTEK, Carlsbad, CA 690–950 nm and 1200–2400 nm, 5–7 ns pulse width, 10 Hz repetition rate) with pulse-to-pulse switching function and an Nd:YAG laser (using the fourth harmonic output, 266 nm, 5–8 ns pulse width, 10 Hz repetition rate, Surelite, Continuum, San Jose, CA) were integrated into the same light path and coupled into the fiber optic diffuser. This study employed illumination at 1220 nm, 1370 nm, 800 nm, and 266 nm to target lipids, collagen, total hemoglobin, and cell nuclei, respectively, in the prostates. 800 nm measurement is insensitive to the blood oxygenation and, therefore, was selected for imaging the total hemoglobin content in *ex vivo* prostate in this study. Since the samples were fresh and intact, and the experiment was started immediately after the operation, we believe there was hemoglobin content remained in the sample, although the hemoglobin may have been deoxygenated. 266 nm illumination targets the contrast of cell nuclei [18,19]. Since the tissue architecture described in the Gleason scoring system of PCa is formed by cancer cells, PASA at 266 nm is a direct measurement of the tissue architectures. We have successfully differentiated the PCa stages in mice prostates *ex vivo* and *in vivo*, as well as human prostate tissues *ex vivo* [9,14]. In this setup, the optical energy at the surface of the side-view window of the needle PA sensing probe was 3.3 mJ at 1220 nm, 1370 nm, 800 nm, and 0.9 mJ at 266 nm. According to our previous paper [14], the sampling volumes for each wavelength were carefully compensated by the emission energy at each wavelength. We estimated

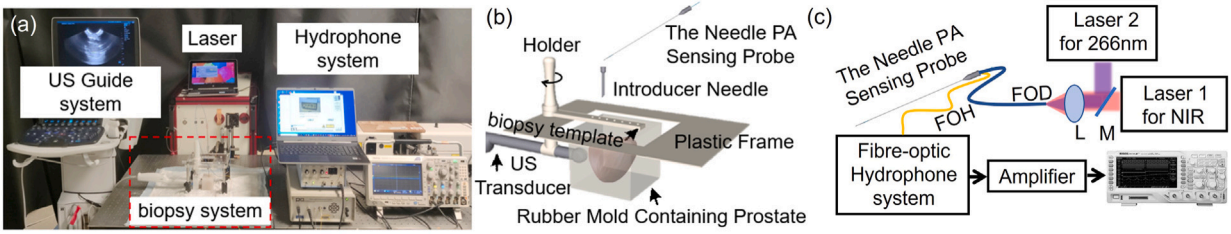

Fig. 2. Experiment setup simulating transperineal TRUS guided biopsy. (a) Overview of the setup. (b) Detailed illustration of the experiment components in the red dashed box in (a). (c) The controlling diagram of the transperineal needle PA sensing probe system. L: Convex len. M: Mirror. FOH: Fiber optic hydrophonr. FOD: Fiber optic diffuser. NIR: Near-infrared.

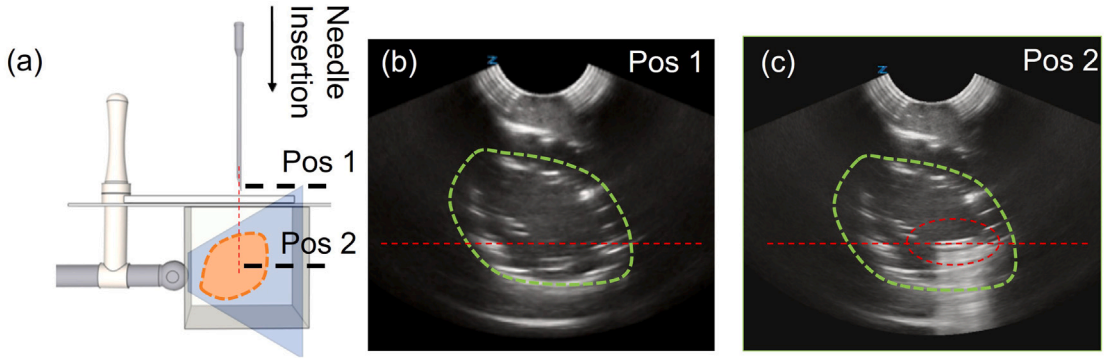

Fig. 3. TRUS guided insertion of the needle PA sensing probe. (a) is the schematic of the US guide system for needle inserting procedures. The US images (b) and (c) were taken before and after the needle insertion, respectively. The needle was marked in the red circle in (c). The red dotted line in (a–c) represents the inserting direction.

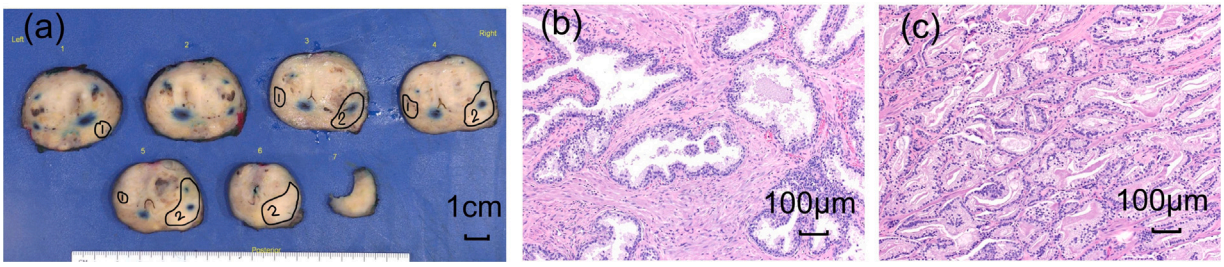

Fig. 4. Histopathology of the intact prostates. (a) Gross pathology of the prostate by slicing the prostate into 4–5 mm thick samples. The blue spots are the spatial markers of the PA measurements by dye injection. The 2D contours of the cancerous regions were delineated in black. (b–c) represent the histology photos of the benign and the cancerous regions. 10× objective magnification.

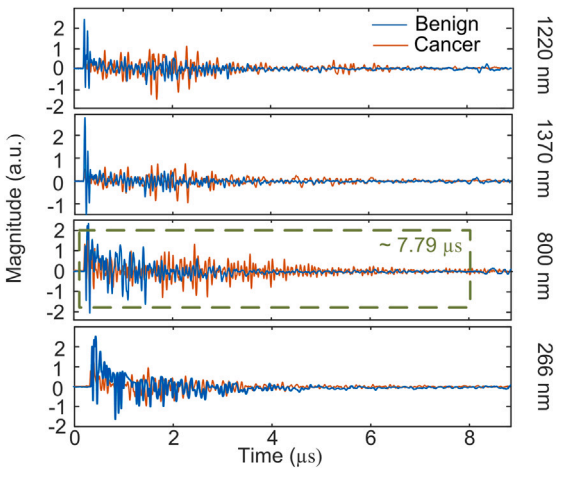

Fig. 5. Example PA signals acquired at 1220 nm, 1370 nm, 800 nm and 266 nm wavelengths for insertions in the benign and cancer regions in an intact human prostate. The orange curves are the measurements in the cancerous region and the blue curves are the measurements in the benign region.

the illumination surface as half of the cylindrical surface of the needle, which was OD × π × h/2 = 1.27 × π × 12/2 mm^2 = 23.9 mm^2. Hence, the optical energy density was approximately 13.8 mJ/cm^2 at 1220 nm, 1370 nm, and 800 nm, and 3.8 mJ/cm^2 at 266 nm. These energy levels are lower than the safety limits of 100 mJ/cm^2 at wavelengths larger than 1000 nm, 31.7 mJ/cm^2 for 800 nm, and 4.9 mJ/cm^2 for 266 nm, as established by American National Standard Institute (ANSI). The PA signals captured by the fiber optic hydrophone were amplified by 20 dB (5072 Pulse/Receiver, 1 k–35 MHz, Olympus, Center Valley, PA) and averaged 56 times, then displayed on an oscilloscope and stored in a computer. The needle PA sensing probe was removed after the measurements.

The needle sensing probe track in the prostate was revisited with a syringe containing a 22G needle under the guidance of US imaging. A depth stop was used to ensure that the tip of the needle was positioned at the distal end of the measured range. 0.05 ml Evans blue dye (E2129, Sigma-Aldrich, St. Louis, MO) was injected. During the needle withdrawal, the dye filled the needle track and stained the whole needle insertion track. For each prostate, 3–5 locations were examined.

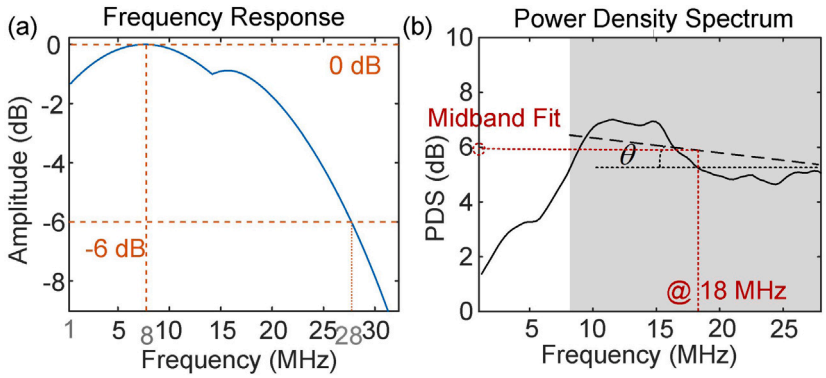

Fig. 6. Method of PASA. (a) The frequency response of the fiber optic hydrophone system. (b) Representative calibrated PA signal power spectrum and PASA analysis. θ represents the linear slope of the PDS in the frequency range from 8 to 28 MHz.

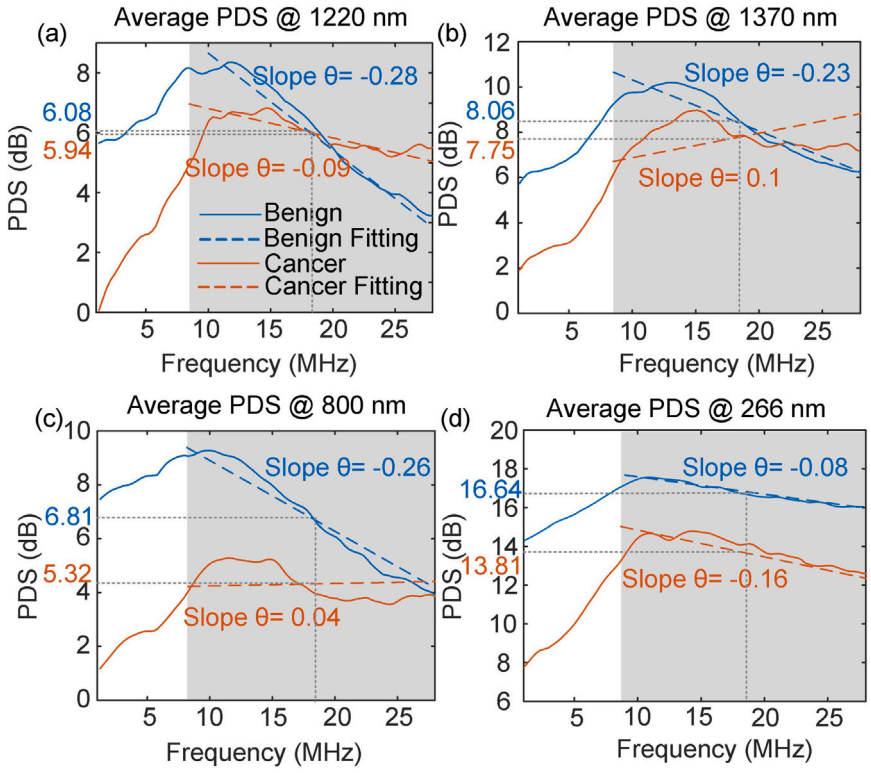

Fig. 7. Averaged PA signal power spectra acquired within the benign and cancerous regions at (a) 1220 nm, (b) 1370 nm, (c) 800 nm and (d) 266 nm and the corresponding linear fits. The blue curves and the orange curves are the average of all measurements within the benign and cancerous regions, respectively. The dashed lines in all images were located at 18 MHz.

2.3. Histopathological examination

After the PA measurements, the intact prostates went through routine histological processing. Each prostate was dissected into 7 to 9 slices along the apex-base orientation. The malignant regions in each slice were identified and marked in the gross photo, as shown in Fig. 4(a). The needle insertions were intentionally oriented perpendicular to the sliced planes. The stained spots in Fig. 4(a) are the locations where needle track intersected with the sliced planes. Considering that the thickness of the slices is around 4–5 mm and the window exposing the optical components are 12 mm long, the histological gradings within the last three slices before the staining disappeared were utilized to compare to the interstitial PA measurements. To accurately differentiate the measurements acquired in the cancerous and benign regions, only the signals acquired more than 2 mm away from the cancer boundaries were included in the statistical analysis. Table 1 summarizes the diagnoses of all the samples included in the statistical analysis.

Table 1
Disease conditions of the sampled locations.

Groups	Sample number @ 1220 nm, 1370 nm, 800 nm	Sample number @ 266 nm
Benign	28	22
Cancer	21	15

2.4. Quantitative analysis with PASA

Fig. 5 shows the representative PA signals acquired at 1220 nm, 1370 nm, 800 nm and 266 nm in a benign and a cancerous region, respectively. The analyzed signal lengths were approximately 8 μs in

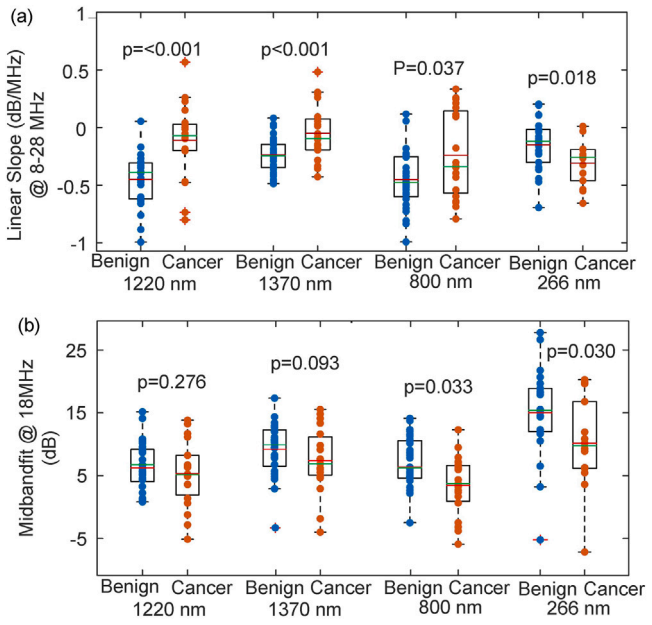

Fig. 8. Statistics of the PASA quantifications, including (a) the linear slope and (b) the midbandfit for the spectral range of 8–28 MHz, for the benign and the cancerous regions at 1220 nm, 1370 nm, 800 nm, and 266 nm. The green line and the red line in each box represent the median and the average, respectively. The upper and lower limits of the boxes are 75 and 25 percentiles of the data distribution.

time and 12 mm in distance (with speed of sound at 1540 m/s), which corresponds to the dimension of the side-view window in the needle probe. The signal power spectra were calculated and calibrated by the frequency domain response of the fiber optic hydrophone in Fig. 6(a). Fig. 6(b) shows a representative PA signal power spectrum after calibration.

As shown in Fig. 6(a), the highest frequency response of the fiber optic hydrophone occurs at 8 MHz and the magnitude of the response drops by 6 dB, i.e. 50%, at 28 MHz. The representative signal power spectrum shows an approximately monotonic descending trend in the 8–28 MHz range. We quantified the magnitude and the frequency component distribution in the spectra using the slope and midbandfit of the linear fit to the spectra in the range of 8–28 MHz. As previously discovered [20,21], a larger spectral linear slope indicates larger high frequency components compared to low frequency ones and vice versa. A larger midbandfit indicates higher content of the corresponding tissue component.

2.5. Statistics and multivariate analysis

Due to the limited sample size, this study focused on differentiating the benign and cancerous regions using the PASA quantifications. T-tests were performed using the built-in function, "ttest", in MATLAB (R2018b, Mathworks Inc., Natick, MA). The null hypothesis is that the PASA of the measurements acquired by the translational needle PA sensing probe cannot distinguish between the benign and the cancerous regions in intact human prostates.

Following the t-tests, the multivariate support vector machine (SVM) was used to differentiate the PASA quantifications acquired from the benign and the cancerous regions using the PA measurements at 1220 nm, 1370 nm, and 800 nm. The measurements at 266 nm were excluded because part of the samples do not have measurements at this wavelength. Fitcsvm, a built-in SVM function in MATLAB, was used with a Gaussian kernel and a box constraint value of 5 to achieve low overfitting while accounting for the high cost of penalty. A 5-fold cross-validation method used in our previous study was implemented, where 80% of the samples was used as training set in turns and the remaining 20% was used for testing [22]. The testing accuracy was calculated as the average of all 5 testing cycles.

3. Result

3.1. PASA at individual wavelength

Fig. 7 shows the averaged PA signal power spectra and the linear fits for all the benign and the cancerous insertions at the wavelengths of 1220 nm, 1370 nm, 800 nm and 266 nm, respectively. Since the fiber optic hydrophone is less sensitivity to low frequency components [16] compared to piezoelectric hydrophone, the PA signal spectra in this study contain less low frequency components compared to our previous study [8,16].

In Fig. 7, at approximately 18 MHz, the signal power spectra of the cancerous group at both 1220 nm and 1370 nm, targeting lipid and collagen contents in the prostate, respectively, intersect with that of the benign group. Larger high-frequency signal components in the cancerous group lead to the larger spectral slopes compared to the benign region, indicating the reduced dimensions of the microarchitectures formed by lipid and collagen. Furthermore, the midbandfits of the cancerous group are slightly lower than those of the benign group, although no significance is shown. The low midbandfit values reflect the decrease of lipid and collagen contents in the cancerous regions. Considering that the connective tissue in the prostate is rich in lipid and collagen contents, these observations are consistent with previous studies where the connective tissues [23] and collagen [24] contents are lower in cancerous prostates.

The measurements at 800 nm targeting the total hemoglobin content show larger spectral slopes and smaller midband-fits in the cancerous group. Larger spectral slope (smaller absolute values as most of the spectra show descending trend) was observed in PCa by our and other groups [8,10]. The midbanfit at 800 nm is lower in the cancerous region. This agrees with a previous study reporting that blood flow decreases in prostate tumor [25].

At 266 nm, the broadband fiber optic hydrophone detected the high frequency signal components generated by the thin layer of epithelium cells in benign prostate tissues [9]. Therefore, the benign group shows high spectral slopes compared to the cancerous group where cancer cells form clusters with large dimensions. The fiber optic hydrophone has limited sensitivity to low frequency components. The low frequency signal components in the cancerous tissue were under-represented in the PASA quantification. As a result, the midbandfit of the cancerous group is lower than the benign group.

Fig. 8 shows the results from the statistical analysis comparing the quantified PASA parameters from the benign and the cancerous regions at the four wavelengths. By performing the t-tests, the linear slope at each of the wavelength can differentiate the two groups with statistical significance, while the midbandfits at 800 nm and 266 nm can also differentiate the two groups with statistical significance. The midbandfits at 1220 nm and 1370 nm also show some difference between the two groups but no statistical significance.

3.2. Multivariate analysis using SVM

Since 266 nm measurements were not acquired in some of the samples, the multivariate analysis does not include the PASA quantifications at 266 nm. Fig. 9 shows the scattered plot of all PASA values at 1220 nm, 1370 nm and 800 nm. The data points show differentiable clustering patterns. The decision surfaces in Fig. 9 were calculated using all the 49 measurements at the three wavelengths. The accuracy of the decision surface in separating the benign and the cancerous regions is 92%. Table 2 lists the accuracy of SVM classification with the measurements at individual wavelength and combined wavelengths using the 5-fold cross-validation approach described in the method section. The highest classification accuracy was achieved by combining the PASA measurements at all the three wavelengths.

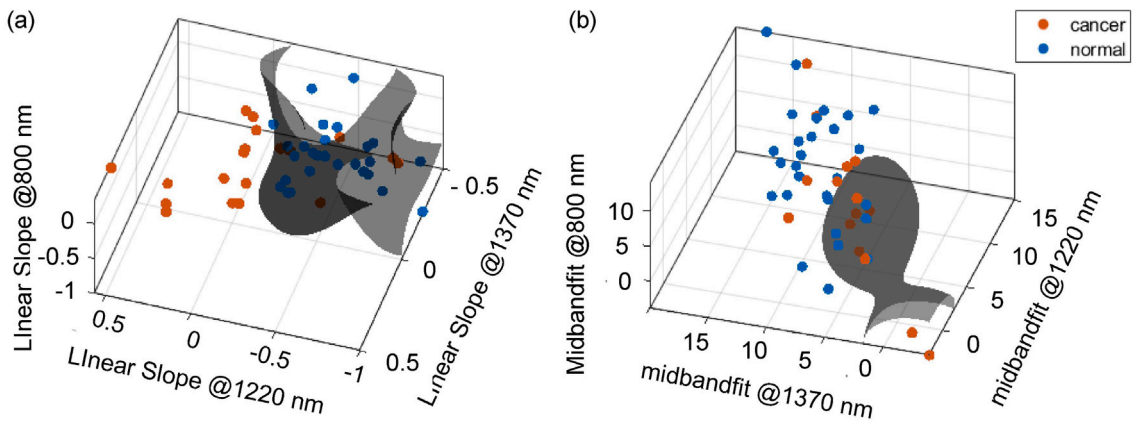

Fig. 9. SVM based categorization between the benign and the cancerous groups at the wavelengths of 1220 nm, 1370 nm, and 800 nm using 49 measurements for the parameter of (a) linear slope and (b) midbandfit.

Table 2
The SVM statistical results using single wavelength or combined wavelengths. (5-fold cross validation, 80% learning, 20% testing).

Wavelength (nm)	1220	1370	800	266	1220, 1370, 800
Spectral slope (dB/MHz)	0.81	0.600	0.60	0.71	0.86
Midbandfit (dB)	0.67	0.67	0.77	0.57	0.80
Both	0.71	0.71	0.71	0.67	0.88

4. Discussion

In the simulation setup, a forward looking endocavity US array was used, although a side-viewing endocavity US array is commonly used in transperineal prostate biopsy. To match the US imaging field-of-view to that in the actual biopsy procedure, a 90-degree probe holder was fabricated. The translational needle PA sensing probe, with a diameter tightly fit to the introducer needle, was always oriented perpendicular to the central line of the convex US array surface. In US imaging, this orientation guarantees a robust reflection signal, which helps the operator in accurately positioning the needle probe. Furthermore, there is a marker along the entire needle body indicating the orientation of the measurement window which helps in matching with histologic diagnosis.

With dye injection following the PA measurements, we successfully correlated the PASA quantifications with the pathological diagnosis at each sampled location. The needle PA sensing probe is only capable of 1D measurements [14]. Measurements taken close to the cancer boundaries were excluded from the statistical analysis because these measurements may contain unresolvable spectral characteristics of both benign and cancerous tissues. In future studies, we plan to investigate uniform sampling and estimating the volume of a cancerous region by the distribution of the PASA quantifications. Considering the large sampling volume provided by the needle PA sensing probe, we may be able to cover the whole prostate volume with limited number of needle probe insertions.

Compared to the piezoelectric hydrophone in our previous studies [8,9], the broadband fiber optic hydrophone significantly extended the frequency range in PASA. As shown in a pilot study [26], describing the histopathological diagnosis of PCa, i.e. Gleason scoring system, the dimensions of the cancer cell clusters are in the range of 10 s to 100 s of microns, which were covered by the frequency range of the fiber optic hydrophone in this study. Fine microscopic tissue architectures correlated to high frequency signal components, such as the thin layer of epithelium cells in benign prostate glands and connective tissues in cancerous regions, were resolved. The decrease in collagen and lipid content can also be observed using the midbandfit parameter, but with relatively low significance when compared to slope. The histopathologic diagnose of PCa is based on tissue architecture rather than tissue content. Therefore, slope representing the tissue architecture is a more reliable parameter in this study compared to the midbandfit, which represents the content of a certain tissue component. These results agree with our predictions drawn from the results derived from piezoelectric hydrophones [9]. Since slope and midbandfit are two natural derivatives of PASA, we included both in this study. The fiber optic hydrophone with broad frequency range in this study improved the differentiability between the benign and cancerous regions. With limited sample number, we observed overlapping between the benign and cancerous group and we did not examine the correlation between the Gleason grades and the PASA quantifications as did in our previous studies [9,14]. Further studies with larger sample size will help us understand the performance of the interstitial PA measurement approach in assessing the aggressiveness of PCa. We believe that including measurements at another wavelength, i.e 266 nm, will assist in better separating the samples in SVM analysis.

5. Conclusion

In this study, we examined the feasibility of integrating a miniaturized, all-optical needle PA sensing probe in a simulated TRUS guided transperineal biopsy procedure. PASA of the measurements acquired by this translational needle PA sensing probe successfully differentiated between the benign and the cancerous regions in human prostates. This study using intact human prostates *ex vivo* paved the road toward clinical testing of our interstitial all-optical needle PA sensing probe powered by PASA for detecting and assessing the aggressiveness of PCa.

Declaration of competing interest

The authors declare the following financial interests/personal relationships which may be considered as potential competing interests: Guan Xu reports the 14G introducer needle in Fig. 2 was provided by Perineologic, 183 N Centre Street, Cumberland, 21502, Md, USA. Guan Xu reports financial support was provided by National Cancer Institute. Guan Xu reports financial support was provided by National Institute of Diabetes and Digestive and Kidney Diseases.

Data availability

Data will be made available on request.

Acknowledgments

This work was supported by National Cancer Institute [grant 5R37CA22282903]; National Institute of Diabetes and Digestive and Kidney Diseases [grant 1R01DK12568701].

Appendix A. Supplementary data

Supplementary material related to this article can be found online at https://doi.org/10.1016/j.pacs.2022.100418. Transrectal ultrasound guided video of the needle insertion.

References

[1] D. Gleason, G. Mellinger, Prediction of prognosis for prostatic adenocarcinoma by combined histological grading and clinical staging, J. Urol. (2002) 953–958.

[2] A.V. Taira, G.S. Merrick, R.W. Galbreath, H. Andreini, W. Taubenslag, R. Curtis, W.M. Butler, E. Adamovich, K.E. Wallner, Performance of transperineal template-guided mapping biopsy in detecting prostate cancer in the initial and repeat biopsy setting, Prostate Cancer Prostatic Dis. (13) (2010) 71–77.

[3] B. Ehdaie, S.F. Shariat, Magnetic resonance imaging–targeted prostate biopsy: Back to the future, Eur. Urol. 63 (1) (2013) 141–142.

[4] G. Fiard, N. Hohn, J.-L. Descotes, J.-J. Rambeaud, J. Troccaz, J.-A. Long, Targeted MRI-guided prostate biopsies for the detection of prostate cancer: Initial clinical experience with real-time 3-dimensional transrectal ultrasound guidance and magnetic resonance/transrectal ultrasound image fusion, Urology 81 (6) (2013) 1372–1378.

[5] C.M. Moore, N.L. Robertson, N. Arsanious, T. Middleton, A. Villers, L. Klotz, S.S. Taneja, M. Emberton, Image-guided prostate biopsy using magnetic resonance imaging–derived targets: A systematic review, Eur. Urol. 63 (1) (2013) 125–140.

[6] L.V. Wang, S. Hu, Photoacoustic tomography: In vivo imaging from organelles to organs, Science 335 (6075) (2012) 1458–1462.

[7] G. Xu, Z.-X. Meng, J.D. Lin, J. Yuan, P.L. Carson, B. Joshi, X. Wang, The functional pitch of an organ: quantification of tissue texture with photoacoustic spectrum analysis, Radiology 271 (1) (2014) 248–254.

[8] S. Huang, Y. Qin, Y. Chen, J. Pan, C. Xu, D. Wu, W.-Y. Chao, J.T. Wei, S.A. Tomlins, X. Wang, J.B. Fowlkes, P.L. Carson, Q. Cheng, G. Xu, Interstitial assessment of aggressive prostate cancer by physio-chemical photoacoustics: An ex vivo study with intact human prostates, Med. Phys. (2018).

[9] J. Jo, J. Siddiqui, Y. Zhu, L. Ni, S.-R. Kothapalli, S.A. Tomlins, J.T. Wei, E.T. Keller, A.M. Udager, X. Wang, G. Xu, Photoacoustic spectral analysis at ultraviolet wavelengths for characterizing the Gleason grades of prostate cancer, Opt. Lett. 45 (21) (2020) 6042–6045.

[10] S. Sinha, N.A. Rao, B.K. Chinni, V.S. Dogra, Evaluation of frequency domain analysis of a multiwavelength photoacoustic signal for differentiating malignant from benign and normal prostates, J. Ultrasound Med. 35 (10) (2016) 2165–2177.

[11] M.P. Patterson, C.B. Riley, M.C. Kolios, W.M. Whelan, Optoacoustic characterization of prostate cancer in an in vivo transgenic murine model, J. Biomed. Opt. 19 (5) (2014) 1–8.

[12] J.B. Rietbergen, A.E. Kruger, R. Kranse, F.H. Schröder, Complications of transrectal ultrasound-guided systematic sextant biopsies of the prostate: evaluation of complication rates and risk factors within a population-based screening program, Urology 49 (6) (1997) 875–880.

[13] P. Narayana, J. Ophir, On the frequency dependence of attenuation in normal and fatty liver, IEEE Trans. Sonics Ultrason. 30 (6) (1983) 379–382.

[14] L. Ni, J. Siddiqui, A.M. Udager, J. Jo, J.T. Wei, M.S. Davenport, P.L. Carson, J.B. Fowlkes, X. Wang, G. Xu, Characterizing the aggressiveness of prostate cancer using an all-optical needle photoacoustic sensing probe: feasibility study, Biomed. Opt. Express 12 (8) (2021) 4873–4888.

[15] W.-H. Choi, I. Papautsky, Fabrication of a needle-type pH sensor by selective electrodeposition, J. Micro/Nanolithography MEMS MOEMS 10 (2) (2011) 1–4.

[16] J.A. Guggenheim, J. Li, T.J. Allen, R.J. Colchester, S. Noimark, O. Ogunlade, I.P. Parkin, I. Papakonstantinou, A.E. Desjardins, E.Z. Zhang, et al., Ultrasensitive plano-concave optical microresonators for ultrasound sensing, Nat. Photonics 11 (11) (2017) 714–719.

[17] J. Power, M. Murphy, B. Hutchinson, D. Murphy, M. McNicholas, K. O'Malley, J. Murray, C. Cronin, Transperineal ultrasound-guided prostate biopsy: what the radiologist needs to know, Insights Imaging 13 (1) (2022) 1–13.

[18] T.T.W. Wong, R. Zhang, P. Hai, C. Zhang, M.A. Pleitez, R.L. Aft, D.V. Novack, L.V. Wang, Fast label-free multilayered histology-like imaging of human breast cancer by photoacoustic microscopy, Sci. Adv. 3 (5) (2017) e1602168.

[19] D.-K. Yao, K. Maslov, K.K. Shung, Q. Zhou, L.V. Wang, In vivo label-free photoacoustic microscopy of cell nuclei by excitation of DNA and RNA, Opt. Lett. 35 (24) (2010) 4139–4141.

[20] G. Xu, I.A. Dar, C. Tao, X. Liu, C.X. Deng, X. Wang, Photoacoustic spectrum analysis for microstructure characterization in biological tissue: A feasibility study, Appl. Phys. Lett. 101 (22) (2012) 221102.

[21] G. Xu, J.B. Fowlkes, C. Tao, X. Liu, X. Wang, Photoacoustic spectrum analysis for microstructure characterization in biological tissue: analytical model, Ultrasound Med. Biol. 41 (5) (2015) 1473–1480.

[22] G. Xu, Z.-x. Meng, J.-d. Lin, C.X. Deng, P.L. Carson, J.B. Fowlkes, C. Tao, X. Liu, X. Wang, High resolution physio-chemical tissue analysis: Towards non-invasive in vivo biopsy, Sci. Rep. 6 (1) (2016) 16937.

[23] C. Morrison, J. Thornhill, E. Gaffney, The connective tissue framework in the normal prostate, BPH and prostate cancer: analysis by scanning electron microscopy after cellular digestion, Urol. Res. 28 (5) (2000) 304–307.

[24] Y. Pu, W. Wang, G. Tang, R.R. Alfano, Changes of collagen and nicotinamide adenine dinucleotide in human cancerous and normal prostate tissues studied using native fluorescence spectroscopy with selective excitation wavelength, J. Biomed. Opt. 15 (4) (2010) 047008.

[25] I.F. Lissbrant, E. Lissbrant, J.-E. Damber, A. Bergh, Blood vessels are regulators of growth, diagnostic markers and therapeutic targets in prostate cancer, Scand. J. Urol. Nephrol. 35 (6) (2001) 437–452.

[26] D.F. Gleason, G.T. Mellinger, Prediction of prognosis for prostatic adenocarcinoma by combined histological grading and clinical staging, J. Urol. 111 (1) (1974) 58–64.

Linyu Ni is currently a Ph.D. student in Biomedical Engineering at the University of Michigan, Ann Arbor. Her primary research interests are photoacoustic microscopy and clinical applications of photoacoustic imaging.

Wei-kuan Lin received the Bachelor's and Master's degree in physics from National Taiwan University, Taiwan. He is currently working toward the Ph.D. degree in Electrical and Computer Engineering in the University of Michigan. His research interests include photoacoustic imaging, optical sensors design and fabrication, and fiber optics and photonics.

Amy Kasputis, BS, is a Clinical Research Coordinator with Dr. Morgan's lab. She works on several clinical studies, including those advanced prostate cancer patients and the Canary Prostate Active Surveillance Study (PASS), Prostate Cancer Risk Clinic (PCRC), and MiCOPilot studies.

Deborah Postiff received her BS degree from the University of Michigan. She is a skilled technologist responsible for procurement of tissue samples for research from surgical specimens for more than investigators at Michigan Medicine. These surgical specimens range from small specimens (parathyroid) to large complex tumor resections.

Javed Siddiqui, MS, is the Technical Director of Molecular Testing Lab at University of Michigan Center for Translational Pathology. His specialty includes urine PCA3 test for prostate cancer detection and CellSearch Circulating Tumor Cell testing for breast, prostate, and colorectal cancers and the recently developed MyProstateScore test.

Matthew J. Allaway, MD, completed his residency in urology and surgery as well as his internship at West Virginia University. Dr. Allaway earned his Doctor of Medicine degree in osteopathic medicine from Midwestern University and his Bachelor of Science degree from Illinois Benedictine College. He is the Founder and CEO of Perineologic. He has been a practicing urologist at Urology Associates in Cumberland, Maryland for more than 20 years, with a special focus on prostate cancer and female urology.

Matthew S. Davenport is Professor of Radiology and Urology, and Service Chief and Vice Chair in the Department of Radiology at Michigan Medicine. He is an internationally recognized expert on the safety and efficacy of radiographic contrast material. He has served on the U.S. Food and Drug Administration Medical Imaging Drugs Advisory Committee, the National Cancer Institute Clinical Imaging Steering Committee, as Chair of the American College of Radiology's Committee on Drugs and Contrast Media, and Vice Chair of the ACR Commission on Quality and Safety. He is a co-author on national policy statements, has published over 200 manuscripts, was founder of the Michigan Radiology Quality Collaborative, and is a funded investigator. His primary clinical interests include patient safety, high-value care, and urologic imaging.

John T. Wei is Professor of Urology, Medical director of Brighton Center for Specialty Care, and Interim Chief of Urology in Division of Andrology and Urologic Health. His areas of active research are on determining how best to quantify urinary incontinence in a clinical setting, quality of care assessments, assessment of clinical outcomes, biomarker validations, and evaluation of health-related quality of life. His clinical practice is in General Urology with a focus on male voiding problems and prostate cancer early detection.

Jay L. Guo started his academic career at the University of Michigan in 1999 and is currently a professor of Electrical Engineering and Computer Science, with joint appointment in Applied Physics, Mechanical Engineering, Macromolecular Science and Engineering. He has 190 refereed journal publications with over 13,500 citations. Many published works from his lab have been reported by numerous media. His group's research includes polymer-based photonic devices and sensor applications, laser generated ultrasound, organic and hybrid photovoltaics, plasmonic nanophotonics, and roll to roll nanomanufacturing technologies.

Todd M. Morgan, M.D., is a urological surgeon and Chief of Urologic Oncology at Michigan Medicine. Dr. Morgan completed his undergraduate and medical training at Harvard University. He returned to the Northwest in 2003 for his urology residency at the University of Washington, before moving to Nashville for his fellowship training in urological oncology at Vanderbilt University. In addition to being a clinician and surgeon, Dr. Morgan is a translational surgeon-scientist. His research involves developing blood-based tests that can guide precision-based treatments for prostate cancer in real time, and he is principal investigator of two large randomized controlled trials evaluating tissue-based biomarkers in men with localized prostate cancer. Dr. Morgan has been the recipient of Young Investigator Awards from the Prostate Cancer Foundation, Society for Urological Oncology, National Comprehensive Cancer Network (NCCN), and Society for Basic Urology Research. He has served on a number of national guideline committees, such as the AUA Muscle-Invasive Bladder Cancer Guidelines, the AUA Advanced Prostate Cancer Guidelines, the NCCN Prostate Cancer Early Detection Guidelines, The ASCO Localized Prostate Cancer Guidelines, and the ASCO Molecular Markers for Prostate Cancer Guidelines.

Aaron M. Udager is Clinical Associate Professor with the Department of Pathology at University of Michigan. He is also Associate Director of Pathology Physician Scientist Training Pathway and Co-Director of Liquid Biopsy Shared Resource at University of Michigan Rogel Cancer Center. He is a surgical and molecular pathologist with clinical expertise in genitourinary, head and neck, and endocrine pathology. He also leads an independently-funded translational genomics research laboratory focused on the molecular pathology of genitourinary, head and neck, and endocrine neoplasia.

Xueding Wang is Professor at the Department of Biomedical Engineering, University of Michigan, holding an adjunct Professor position at the Department of Radiology. Before working as an independent principal investigator, Dr. Wang received his Ph.D. from the DDwight Look College of Engineering at Texas A&M University, and then finished postdoctoral training at the University of Michigan School of Medicine. Dr. Wang has extensive experience in imaging system development and adaptation of novel diagnostic technology to laboratory research and clinical managements, especially those involving light and ultrasound. Sponsored by NIH, NSF, DoD and other funding agencies, his research has led to over 120+ peer-reviewed publications. At the University of Michigan Medical School, a major part of his research is focused on clinical applications of photoacoustic imaging, including those involving arthritis, prostate cancer, liver conditions, breast cancer, Crohn's disease, and eye diseases. Dr. Wang is the recipient of the Sontag Foundation Fellow of the Arthritis National Research Foundation in 2005, and the Distinguished Investigator Award of the Academy of Radiology Research in 2013. He is also sitting on the editorial boards of scientific journals including Photoacoustics, Journal of Biomedical Optics, Medical Physics, and Ultrasonic Imaging, and being the steering committee member of the Journal of Lightwave Technology.

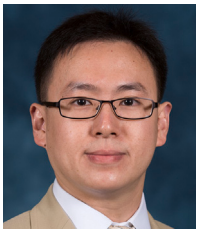

Guan Xu received his PhD and postdoctoral training in optical and ultrasound imaging in biomedicine. He received a predoctoral award from Congressionally Directed Medical Research Programs, a postdoctoral fellowship from American Heart Association, a Career Development Award from American Gastroenterology Association, a Senior Research Award from Crohn's and Colitis Foundation and an R37 MERIT award from National Cancer Institute.